European Journal of Pharmaceutics and Biopharmaceutics 136 (2019) 102–107

Contents lists available at ScienceDirect

European Journal of Pharmaceutics and Biopharmaceutics

journal homepage: www.elsevier.com/locate/ejpb

Research paper

Ultrasound-responsive nanobubbles for enhanced intravitreal drug migration: An *ex vivo* evaluation

Sachin S. Thakur[a,b], Ying-Shan Chen[b], Zachary H. Houston[c], Nicholas Fletcher[c], Nigel L. Barnett[d,e,f], Kristofer J. Thurecht[c], Ilva D. Rupenthal[b,*], Harendra S. Parekh[a,*]

[a] The University of Queensland, School of Pharmacy, Pharmacy Australia Centre of Excellence, 20 Cornwall Street, Woolloongabba, Brisbane, QLD 4102, Australia
[b] Buchanan Ocular Therapeutics Unit, Department of Ophthalmology, New Zealand National Eye Centre, Faculty of Medical and Health Sciences, University of Auckland, Private Bag 92019, Auckland 1142, New Zealand
[c] Centre for Advanced Imaging (CAI), Australian Institute for Bioengineering and Nanotechnology (AIBN) and ARC Centre of Excellence in Convergent BioNano Science and Technology, The University of Queensland, Brisbane, QLD 4072, Australia
[d] Clem Jones Centre for Regenerative Medicine, Faculty of Health Science & Medicine, Bond University, Gold Coast, QLD 4229, Australia
[e] Queensland Eye Institute, 140 Melbourne Street, South Brisbane, QLD 4101, Australia
[f] The University of Queensland, UQ Centre for Clinical Research, Building 71/918 RBWH Herston, Herston, QLD 4029, Australia

ARTICLE INFO

Keywords:
Ultrasound
Nanobubbles
Intravitreal drug delivery
Ocular drug delivery
Ex vivo

ABSTRACT

The intravitreal route faces many challenges in rapidly and effectively reaching posterior eye pathology, with administered therapeutics experiencing non-specific distribution around and premature clearance from ocular tissues. Nanobubbles and ultrasound may improve outcomes of intravitreally administered drugs by influencing the directionality of drug-containing particle migration. In this study, we assessed the impact of trans-scleral or corneal ultrasound application on the distribution of intravitreally-injected nanobubbles. Rhodamine-tagged gas entrapped nanobubble formulations were prepared and injected into *ex vivo* bovine and porcine eyes and subjected to ultrasound (1 MHz, 0–2.5 W/cm^2, 50–100% duty, 60 s). Bovine eyes were partially dissected to visualize the vitreous humor and particle migration was evaluated via optical fluorescence spectroscopy. Directional migration in porcine eyes was evaluated using a snap freezing protocol complemented by quantification of regional fluorescence. The impact on nanobubble migration following pars-plana injection and sequential ultrasound cycle application from scleral or corneal-surface positions was also assessed. Administration of ultrasound significantly enhanced the directional migration of nanobubbles in both *ex vivo* models, with multiple corneal ultrasound cycles promoting greater migration of dye-filled nanobubbles to posterior regions of the vitreous. Moreover, particles moved in a directional manner away from the ultrasound wave source demonstrating an ability to effectively control the rate and path of nanobubble migration. These findings establish an encouraging new and safe modality enabling rapid distribution of intravitreally-injected therapeutics where expeditious therapeutic intervention is warranted.

1. Introduction

Diseases of the posterior eye pose an immense burden on global healthcare systems [1,2]. Age-related macular degeneration (AMD), diabetic retinopathy (DR) and glaucoma are three such examples, with each being listed among the top 10 priority eye diseases by the World Health Organization [3]. At present, treatment options for these diseases are limited; late stage AMD and DR are treated with intravitreal injections of antibody-based therapeutics typically administered every 4–6 weeks [4,5] whereas glaucoma is managed by intraocular pressure lowering eye drops [6]. In all cases, the delivery of treatments to the target tissue has been sub-optimal.

A substantial factor limiting therapeutic efficacy is the location of posterior eye pathologies. These diseases affect numerous layers of the

Abbreviations: 5-TAMRA, 5-carboxy-tetramethylrhodamine *N*-succinimidyl ester; AMD, Age-related macular degeneration; DPPC, 1,2-dipalmitoyl-*sn*-glycero-3-phosphocholine; DR, Diabetic retinopathies; DSPE-PEG(2k)-OMe, 1,2-distearoyl-*sn*-glycero-3-phosphoethanolamine-N-[methoxy(polyethylene glycol)-2000]; PFP, Perfluoropropane

* Corresponding authors at: Pharmacy Australia Centre of Excellence, School of Pharmacy, The University of Queensland, Brisbane, Queensland 4072, Australia (H.S. Parekh).
E-mail address: h.parekh@uq.edu.au (H.S. Parekh).

https://doi.org/10.1016/j.ejpb.2019.01.014
Received 8 November 2018; Received in revised form 14 January 2019; Accepted 15 January 2019
Available online 17 January 2019
0939-6411/

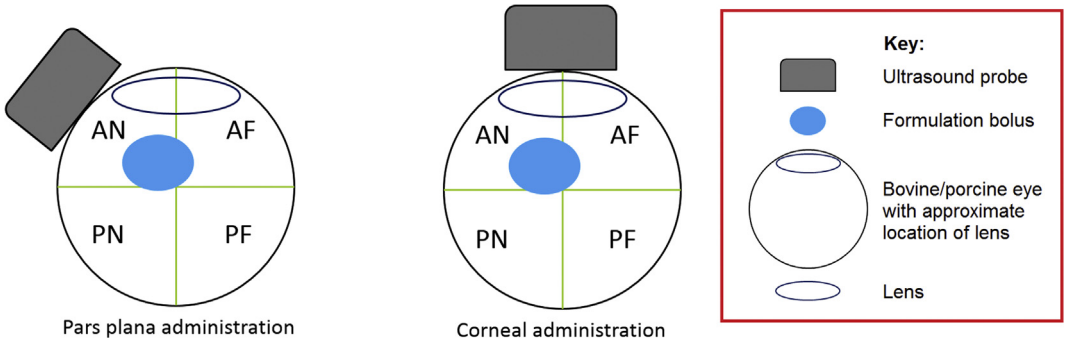

Fig. 1. Schematic depicting investigated modes of therapeutic ultrasound administration to the bovine and porcine eye. The lens of the eye has been included to clarify the orientation of the ultrasound probe and injected formulation bolus in relation to the other ocular structures. The vitreous was divided in four sections in relation to the site of injection and bolus; AN = anterior near, AF = anterior far, PN = posterior near, PF = posterior far. The near regions correspond to the temporal side of the eye whereas the far regions correspond to the nasal side of the eye. Probe size not to scale.

retina and although intravitreal drug delivery can attain a higher dose of therapeutic in these layers when compared to other conventional ophthalmic routes [7,8], still only a fraction of the administered dose reaches its target [9]. This is due to the influence of convective flow [10,11], non-specific diffusion [12] and saccade [13,14] on drug migration, with each of these factors hastily displacing the injected bolus. While it has been proposed that injecting therapeutic closer to the target site via deeper injection will enhance migration towards and uptake by target tissue [15], this remains controversial due to the heightened risk of permanent tissue damage.

Ultrasound-facilitated drug delivery has received increased interest due to its ability to enhance permeation of therapeutics through various biological barriers [16]. The technique has been safely used on ocular tissue, demonstrating an ability to enhance therapeutic permeation through both the cornea [17] and sclera [18]. In addition, preliminary studies have also investigated the technique as an adjunct to improve intravitreal drug migration. Here, the therapeutic is first injected into the vitreous together with an ultrasound-responsive contrast agent, such as micro- or nanobubbles, after which ultrasound is administered to the sclera of the eye (Fig. 1). The contrast agent enhances the effect of the stimulus (be this cavitation or streaming) in a localized manner enabling the ultrasound to be used at low, biologically safe intensities. To date this technique has shown immense potential in improving ocular drug outcomes in small animal (rat) models [19,20], although no reports currently exist showing it as a useful approach in larger animals whose eyes more closely resemble the dimensions and geometry of the human eye.

In order to successfully implement the approach in the clinical setting, it is imperative to first study its effects in large animal models. As *in vivo* models incur sizeable cost and ethical issues on such evaluations, a prudent initial approach is to exploit freshly excised *ex vivo* eyes to understand and optimize the strategy. Moreover, *ex vivo* models offer greater insight beyond cell culture into potential physical and, in certain cases, biochemical barriers that a therapeutic or drug delivery system may face in reaching its target. The *ex vivo* eye is now established as a robust model for therapeutic evaluations, with various biological structures retaining their properties for many hours following animal sacrifice [21–24].

In this study, ultrasound was used to influence the migration of nanobubbles in *ex vivo* vitreous humor. Studies evaluating the feasibility of the technique were initially performed and optimized using the larger *ex vivo* bovine eye, then transitioned to porcine eyes whose dimensions closely resemble those of humans.

2. Experimental section

2.1. Materials

1,2-dipalmitoyl-sn-glycero-3-phosphocholine (DPPC) and 1,2-distearoyl-sn-glycero-3-phosphoethanolamine-N-[methoxy(polyethylene glycol)-2000] (DSPE-PEG(2k)-OMe) were purchased from Avanti® Polar Lipids (Alabaster, AL, USA). Perfluoropropane (PFP) was purchased from Coregas (Darra, QLD, Australia). 5-carboxy-tetramethylrhodamine *N*-succinimidyl ester (5-TAMRA) was purchased from Okeanos Tech Co., Ltd. (Beijing, China).

2.1.1. Bovine eyes

The bovine eye was used as the benchmark model for evaluations as it could be sourced immediately post-mortem on a regular basis. Eyes were purchased from Teys Australia™ (Beenleigh, QLD, Australia). All experiments were performed within 8 h of sacrifice of the animal.

2.1.2. Porcine eyes

Given their restricted availability, porcine eye evaluations were conducted following completion of bovine eye optimization studies. Eyes were sourced from Pork Mart and Poultry (Greenlane, New Zealand). Due to the unavoidable aged nature of tissue (received 24 h post-mortem), studies on ocular structures including the cornea, lens, sclera and retina were not performed. However, studies upon the vitreous humor were possible with this model as the humor retains its structural and mechanical properties for up to 60 h post-mortem [22,23].

2.2. Preparation of tagged nanobubbles

Formulations were prepared as previously described [25,26]. Briefly, DPPC, DSPE-PEG(2k)-OMe and 5-TAMRA (92:6:2 M ratio) were added to a round bottom flask and dissolved in chloroform. The flask was then mounted onto a rotary evaporator and the solvent was removed by heating under vacuum at 65 °C and 100 rpm to obtain a thin film. Next the film was hydrated with phosphate buffered saline (PBS, pH 7.4) to obtain a crude liposome mixture. This mixture was downsized using bath sonication and subsequently placed in an air evacuated crimp sealed vial. PFP was added to the vial using a gas tight syringe, pressurising the liposomes, which facilitated entrapment of the contrast agent. The vials were vigorously shaken under heat to ensure gas entrapment into the particles could be maximised. This process resulted in the formation of crude nanobubbles. The formed nanobubbles were further downsized by gas-tight extrusion through 400 nm polycarbonate membranes (Avanti® Polar Lipids, Alabaster, AL, USA). Following extrusion a residual foam layer was observed on the formulation. This layer was discarded to remove large particles and ensured

only true nano-sized particles were used in the study. Extruded and crude (unextruded) nanobubbles were characterized to identify differences in their size and polydispersity using a Zetasizer Nano ZS (Malvern Instruments, Malvern, UK). Finally, echogenicity of both particles was evaluated using an Ellex® EyeCubed imaging ultrasound unit equipped with a 10 MHz sealed probe set to B-Scan mode (25 fps) [26], and quantified by derivation of the Mean Grayscale Value of the image using Adobe Photoshop CC (14.2).

2.3. Intravitreal injection and therapeutic ultrasound administration technique in large mammal eyes

An insulin syringe equipped with an 8 or 12.7 mm 30G needle was used for nanobubble injection into porcine and bovine eyes, respectively. A clinically relevant maximum volume of 100 µL was injected through the pars plana located at the temporal side of the eye. A slow injection speed (~3 s) was adopted to minimize uncontrollable distribution, with appropriately injected formulations manifesting as boluses posterior to the lens. Extraocular ultrasound (JUS-2, Johari® Digital, Jodhpur, India) was applied (1 MHz, 50% [porcine] or 100% [bovine] duty, 2.5 W/cm^2, 60 s) using a 34 mm flat head probe via either the pars plana or cornea of the eye (Fig. 1).

2.4. Evaluations of ultrasound-triggered particle movement in large mammal eyes

2.4.1. Visual and optical fluorescence imaging

An adapted partial dissection technique was employed to visualize the vitreous humor in bovine eyes [27]. Briefly, a defined section of the sclera located on the nasal side of the eye was excised to reveal the vitreous body. While keeping the vitreous humor intact, an artificial seal was prepared by affixing the opened portion of the eye to the lid of a P10 petri dish using cyanoacrylamide glue. Injected formulations could be visually observed through the prepared window.

Optical fluorescence evaluations were employed to quantify intravitreal propagation of nanobubbles. Particle migration in the presence and absence of ultrasound was observed using an In-Vivo MS FX PRO imaging apparatus (Bruker, Billerica, MA, USA) at 530 nm Ex/590 nm Em with 15 s exposure and 190 mm field of view to allow simultaneous imaging of control and treatment eyes. Following image capture, eyes were demarcated into anterior and posterior hemispheres (as in Fig. 1; AN + AF = anterior hemisphere, PN + PF = posterior hemisphere), and the proportion of nanobubble dose in either hemisphere before and following ultrasound application was quantified using ImageJ software. As unilateral movement was being evaluated, only the corneal administration strategy was investigated in this evaluation.

2.4.2. Porcine eye snap freezing evaluations

An adaptation of the whole globe snap freeze technique was used to quantify the extent of ultrasound-facilitated therapeutic migration around the porcine eye [28,29]. Briefly, following intravitreal injection of dye and subsequent ultrasound administration, the whole eyeball was appropriately oriented and snap-frozen in liquid nitrogen.

Following complete freezing, the eye was first divided across the equator and subsequently into nasal and temporal segments in order to obtain four distinct regions (as specified in Fig. 1). Vitreous humor was collected from each region into Eppendorf® tubes and samples were centrifuged at 16,000*g* for 25 min at 4 °C to sediment the collagen and any residual retinal material. Nanobubbles and 5-TAMRA readily separated from collagenous regions of the vitreous humor by centrifugation and no further extraction steps were necessary. The supernatant was collected and 5-TAMRA concentrations were evaluated by fluorescence (530 nm Ex/590 nm Em) using calibration curves prepared on the same day.

See supplementary information for bovine and porcine tissue dissection technique, ultrasound administration strategies used and intraocular nanobubble stability profile.

2.5. Histological evaluations

Any potential ultrasound-induced damage to *ex vivo* bovine tissue was assessed using histology. Tissue was fixed immediately following ultrasound application in 10% formalin for 72 h followed by dehydration in 70% ethanol for 24 h. Overnight de-fatting and clearing steps with ethanol (70%, 90%, 95%, 3x 100%; 1 h each) and xylene (30 min, 30 min, 40 min) were conducted before paraffin wax infiltration (1 h, 1.5 h, 1.5 h) and tissue embedding within a wax block. A microtome was used to obtain 4 µm tissue sections which were placed on non-charged slides for staining. Gross damage to both anterior and posterior structures was evaluated using haematoxylin and eosin (H&E) staining.

2.6. Statistical analysis

All values are shown as mean ± SD following experiments carried out using $n \geq 3$ independent samples unless clearly stated otherwise. A Shapiro-Wilk normality test was conducted to confirm the obtained data was normally distributed. Comparisons among groups were conducted using one-way or two-way ANOVA which featured a Dunnett's multiple comparisons post-test, with $p < 0.05$ being considered statistically significant.

3. Results

3.1. Extrusion processes improve nanobubble size distribution and gas entrapment

While protein-based nanobubbles have previously been prepared with minimal size variation [30], robust protocols are not currently in place to achieve the same with lipid-based bubbles. Extrusion has been routinely used for liposomal/lipid nanoparticle downsizing and size standardization and its use in this evaluation achieved the same effect. Extruded nanobubbles demonstrated a *Z*-average size of 205.0 ± 35.3 nm and a polydispersity index of 0.331 ± 0.095. In contrast, crude nanobubbles were both larger (*Z*-average size: 606.4 ± 132.4 nm) and more heterogenous (polydispersity index: 0.496 ± 0.096). Surprisingly, the shear forces offered by extrusion also enhanced formulation echogenicity. A 12 µg/ml aliquot of extruded nanobubbles was approximately 3-fold more echogenic than the same concentration of crude nanobubbles (Fig. 2). Additionally at this dilution, extruded nanobubbles were able to retain 71.6 ± 6.6% of their echogenicity over 30 min, while the crude nanobubbles could only retain 26.4 ± 3.5% of their echogenicity. Finally, complete loss of

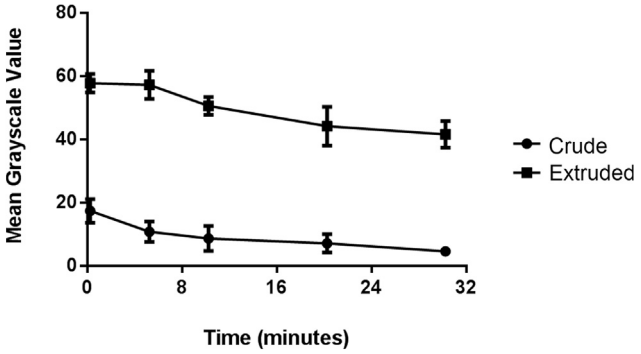

Fig. 2. Impact of gastight extrusion on the 30 min echogenic profile of DPPC:DSPE-PEG(2k)-OMe nanobubbles in PBS (pH 7.4). Signals correspond to 600 µg (100 µL) of lipid dispersed in 50 mL of PBS, with measurements being taken from grayscale image provided by Ellex® EyeCubed ultrasound system. A higher grayscale value corresponds to a greater in-formulation gas content.

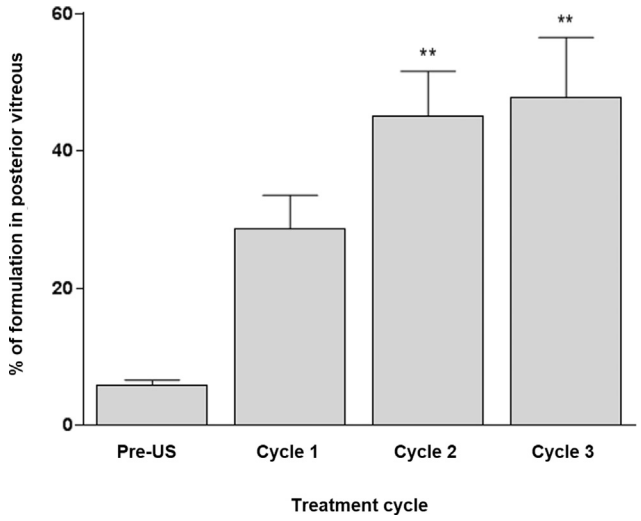

Fig. 3. Migration of rhodamine nanobubbles into posterior regions of bovine vitreous following three cycles of corneal ultrasound administration (1 MHz, 100% duty, 2.5 W/cm^2, 60 s). Sixty second long cycles were administered 2, 5, and 8 min following injection. Tissue was demarcated into anterior and posterior regions and the fluorescence intensity in each was compared to provide the percentage of formulation that had reached the posterior vitreous. Differences in formulation concentrations were analyzed using one-way ANOVA.

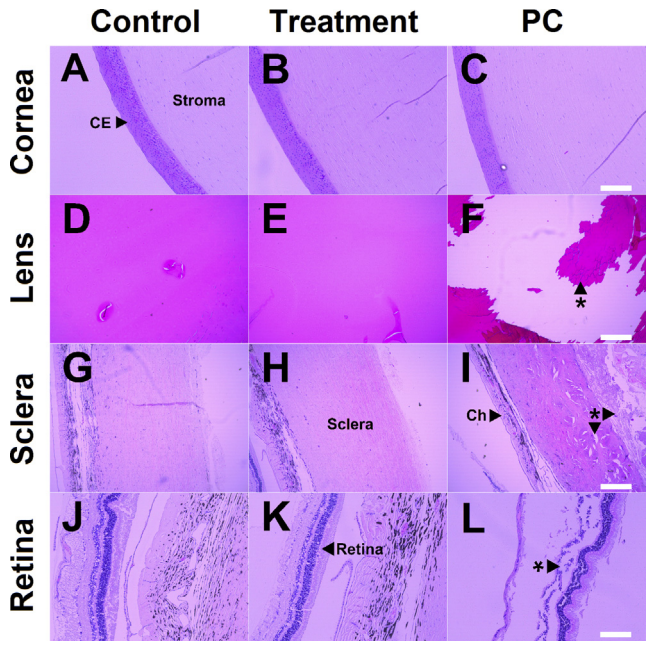

Fig. 4. Sample images from histological evaluations demonstrating the impact of ultrasound exposure (1 MHz, 100% duty, 2.5 W/cm^2, 60 s) on ocular tissues in comparison to healthy (control) and damaged (ultrasound administration prolonged to 240 s, PC) tissue. In the case of cornea and lens sections ultrasound was administered in a transcorneal fashion, whereas in the case of sclera and retina sections it was administered in a trans-scleral fashion through the pars plana. Damage clearly visible in panels F, I and L has been identified using an asterisk*. Scale bar = 400 μm for sclera sections, 200 μm for all other sections. Key: CE = corneal epithelium, Ch = choroid, PC = positive control.

echogenicity was observed when either nanobubble formulation was exposed to therapeutic JUS-2 ultrasound.

3.2. Ultrasonic cycles can migrate nanobubbles in bovine vitreous

Nanobubble movement in the vitreous could be readily visualized using the employed optical fluorescence setup. Over the timeframe studied, no particle migration was observed in absence of ultrasound administration. Conversely, application of corneal ultrasound (1 MHz, 100% duty, 2.5 W/cm^2, 60 s) significantly promoted nanobubble migration towards the posterior segment ($p < 0.001$, Fig. 3). Three cycles of 60 s ultrasound exposure were each separated by 2 min to minimize the hyperthermic effects of the stimulus on the tissue. Using this protocol, it was observed that each additional cycle increased bulk transfer of the formulation into the posterior hemisphere of the vitreous humor. Region of interest analysis revealed that following bolus administration, < 10% of the administered dose was present in the posterior half of the vitreous humor in all cases prior to ultrasound application (Fig. 3). A single cycle of ultrasound resulted in an approximate 200% increase with 28.6 ± 8.5% of the dose rapidly transferring to the posterior region. Moreover, this transfer could be further increased by multiple cycles with 45.1 ± 11.4% and 47.8 ± 15.2% of the dose reaching the posterior vitreous after 2 and 3 ultrasonic cycles, respectively ($p < 0.01$). Ultrasound was separately also administered to native dye and non-echogenic dye-containing liposomes injected into the vitreous humor. In both these cases, the stimulus had no impact on particle migration (data not shown).

3.3. Impact of ultrasound on integrity of the ex vivo bovine eye

Histological analysis revealed that optimized ultrasonic parameters had no identifiable impact on the integrity of any of the evaluated tissues, whether ultrasound was applied to the eye via the cornea or the sclera (Fig. 4). The duration of ultrasound was extended to 240 s to assess whether this would affect tissue integrity and serve as a positive control (PC). Under these vastly exaggerated ultrasound application conditions damage was evident on regions of tissue adjacent to the probe application point following the prolonged corneal or pars plana administration; in the case of corneal ultrasound administration central clouding of the lens was observed whereas pars plana ultrasound administration induced substantial tissue dehydration and retinal delamination. Each of these features were readily identified as tissue damage when evaluated using histology (Fig. 4F, 4I and 4L).

3.4. Bolus migration can be evaluated using a snap freezing protocol in the ex vivo porcine eye

The phenomenon of ultrasound-assisted bolus bubble transfer was further investigated in the porcine eye model. Given its similarity in size and physiology to the human eye [31], it was postulated that findings in this model would be considered more clinically relevant.

The snap freeze method was utilized to understand distribution of the formulation inside porcine eyes. An ultrasonic protocol of 1 MHz, 50% duty, 2.5 W/cm^2, 60 s was employed for the porcine eye studies. Similar to the bovine model, particle migration was not observed in the porcine eye via simple convection in the absence of ultrasound. The two investigated ultrasound probe orientations (pars plana and corneal) had starkly contrasting outcomes on the path of nanobubble migration. In the case of pars plana administration, nanobubbles were primarily driven from the AN region into the AF region of the vitreous, with 56.5 ± 8.9% of the injected dose being transferred. This strategy resulted in a significantly greater AF nanobubble concentration than from the other two tested conditions ($p < 0.0001$). In contrast, corneal administration resulted in the greatest proportion of nanobubbles transferring from the AN region into the PN region (36.3 ± 4.2% of injected dose transferred, $p < 0.0001$, Fig. 5). Neither approach elicited significant movement of the formulation to the PF region, which contained < 10% of the administered formulation dose in all instances.

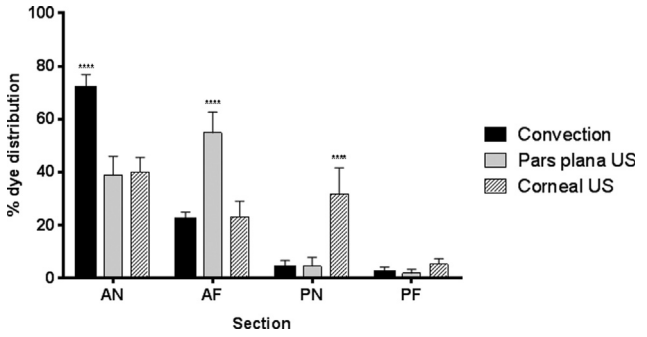

Fig. 5. Distribution of rhodamine nanobubbles following convection, pars plana- or corneal- ultrasound administration. Parameters of 1 MHz, 50% duty, 2.5 W/cm^2, 60 s were used. The vitreous was divided into four sections in relation to the site of injection and bolus; AN = anterior near, AF = anterior far, PN = posterior near, PF = posterior far, US = ultrasound. The near regions correspond to the temporal side of the eye whereas the far regions correspond to the nasal side of the eye. Statistical analysis by two-way ANOVA with Dunnett's multiple comparisons post-hoc test. $^{****}p < 0.0001$ compared with other treatments within same section.

4. Discussion

The primary objective of this study was to determine whether the nanobubble-ultrasound strategy holds potential in facilitating the rapid, directional migration of therapeutics towards their target site in large animal models. Nanobubbles were chosen in place of simple dye or non-gaseous nanoparticles as prior evaluations demonstrated that gas entrapment played an essential role in driving particle responsiveness to ultrasound [26]. With standard formulation strategies failing to produce homogenous nanobubbles, we sought to utilize an extrusion technique to standardize bubble size. While extrusion was able to reduce both particle size and heterogeneity, it unexpectedly also increased gas content and so echogenicity of the resultant nanobubbles. This may be due to extrusion having improved the shell strength of the nanobubbles and therefore allowing these to better retain gas, and for extended periods. In contrast, crude nanobubbles were only subjected to sonication which, while an effective downsizing technique, has previously been reported to form less stable lipid membranes [32]. At present, extrusion processes are not in use for lipid nanobubble manufacture, however, our findings suggest that the technique holds potential in this application. An observed loss of nanobubble echogenicity following therapeutic ultrasound administration also confirmed that in spite of the novel extrusion process, the nanobubbles are still responsive to the applied stimulus. With the extruded nanobubbles demonstrating superior size and echogenic properties, the crude nanobubbles were excluded from subsequent studies.

Following preparation of our nanobubbles, we moved to evaluate their migration behaviour in bovine eyes. This model was an ideal choice for optimization studies due to the immediacy with which they could be sourced post-mortem. Initial observations demonstrated that ultrasound unequivocally migrated our nanobubbles inside the vitreous humor, likely through an acoustic streaming phenomena, which involves the generation of flow currents by sonic/ultrasonic waves within a liquid medium [33,34]. While streaming phenomena have routinely been proposed as a mechanism by which ultrasound encourages cell/tissue internalization of a therapeutic, they have very rarely been proposed for bulk transport of therapeutic through a tissue [35,36], as was observed with our nanobubble formulation. The use of streaming phenomena such as radiation-force in ultrasound-assisted drug migration has been restricted to pushing formulations across micrometre lengths e.g. towards capillary walls [37,38]. Our observations suggest that, given the comparatively stagnant nature of the vitreous humor (*c.f.* blood flow), acoustic streaming may well be an ideal mechanism by which to encourage particle transfer within this and other media. Additionally, in our study, streaming was only observed when using gas-containing nanobubbles with ultrasound having no impact on movement of native dye or non-gaseous dye-containing liposomes, highlighting the importance of gas incorporation for the strategy to work more effectively.

Although particle movement could be qualitatively observed in an intact bovine eye by visual observation through the cornea, surgical manipulation was essential in order to quantify the extent of that movement. Partial eye dissections are routinely employed in experimental procedures as they maintain integrity of the vitreous environment [27,39,40], thus a dissection of this nature was adopted as a direct measure of bubble migration. As the entire vitreous humor is retained within the eye and injection/ultrasound administration is carried out away from the surgically created viewing window, it is expected that findings from these evaluations closely approximate those occurring in an intact eye.

Regulatory guidelines currently in place put strong emphasis on the physiological compatibility of devices administered on/to the eye, notably requiring caution to be exercised when using devices that may increase ocular temperature [41,42]. This factor was important to keep in mind during our evaluation, with ultrasound being well known to dissipate as thermal energy. The tissue was able to withstand 60 s of our employed ultrasound protocol, although increasing the duration caused a visible loss of tissue rigidity. The effects of prolonged exposure (240 s) were clearly visible with histology; while the cornea appeared to withstand prolonged ultrasound, the stimulus severely affected each of the lens, sclera and retina. This provided invaluable information on the maximum duration that the stimulus could be applied using our ultrasound apparatus.

To counter these detrimental effects, we pursued the use of multiple cycles of ultrasound separated by stimulus-free intervals for tissue recovery. This strategy effectively mitigated the adverse potential of ultrasound, while each additional cycle served to further enhance directional bubble migration. As such, adopting a similar strategy when taking this technique forward to maximize the outcomes of ultrasound administration in a safe manner would be prudent.

Comparisons between pars plana and corneal surface-delivered ultrasound in the porcine eye clearly demonstrated that probe orientation greatly impacts the direction of particle movement. This is unsurprising as the direction of a generated acoustic stream will typically be determined by the source of the impulse in the absence of other counter-streams. While particles generally moved in a directional manner away from the applied ultrasound source, it was interesting to note that only a limited quantity of bubbles reached the PF region. This may be due to the heterogenous vitreous restricting particle movement in certain directions [29,43] or constraints brought about by the design of the utilized ultrasound probe/device, although further studies that more precisely characterize ultrasonic wave propagation through the vitreous humor are necessary in order to fully understand the inability to attain PF deposition. As we were only able to measure dye concentrations, it is also unclear whether the observed migration was due to ultrasound propelling the nanobubbles or ultrasound displacing and dispersing the 5-TAMRA from the nanobubbles. It is envisaged that this strategy will be used to assist migration of large therapeutics such as antibodies and peptides, thus it is important in future evaluations incorporate macromolecules into the formulation and assess how ultrasound influences their release from the system and transport toward their target.

Importantly, this study has demonstrated the ability to rapidly migrate highly echogenic nanobubbles to the posterior regions of the vitreous humor. There appears to be immense benefit from being able to do so, with computational models having previously determined that a drug bolus residing closer to the target site in the retina will achieve superior C_{max} and AUC in adjacent retinal tissues [15]. With the end goal being improvements in retinal drug delivery, future studies will look into using the ultrasound/nanobubble approach in an *in vivo* model using a custom-designed ophthalmic ultrasound probe/device.

These studies will also help evaluate how physiological phenomena such as intraocular convection may influence the effectiveness of our strategy. We anticipate that ultrasound will be able to work together with convective flow and further enhance therapeutic migration to the posterior eye. Emphasis should remain on utilizing large animal models with physiological similarities to the human eye in order to attain clinically relevant outcomes.

5. Conclusion

The ultrasound-nanobubble strategy was investigated and optimized in two independent *ex vivo* large mammal eye models. Acoustic streaming was seen as the primary driving factor for ultrasound-assisted intravitreal particle migration, with only gaseous particles being able to migrate under the assessed conditions. Bovine eye studies revealed that repeated cycles of corneal ultrasound could improve the migration of injected nanobubbles deeper into the posterior regions of the vitreous humor while causing no observable acute damage to the ocular tissues. Porcine eye studies demonstrated that the orientation of the applied ultrasound impulse could control the direction of nanobubble migration.

Acknowledgements

The authors would like to thank the Translational Research Institute Histology Facility at the University of Queensland Diamantina Institute for their assistance with the histology experiments.

Declaration of interest

The authors were supported by research and maintenance funds from The University of Queensland and The University of Auckland. SST was supported by an Australian Postgraduate Award. The authors have no other relevant affiliations or financial involvement with any organization or entity with a financial interest in or financial conflict with the subject matter or materials discussed in the manuscript apart from those disclosed.

Appendix A. Supplementary material

Supplementary data to this article can be found online at https://doi.org/10.1016/j.ejpb.2019.01.014.

References

[1] S.P. Mariotti, Global Data on Visual Impairments 2010, World Health Organization, Geneva, Switzerland, 2012.
[2] J. Köberlein, et al., The economic burden of visual impairment and blindness: a systematic review, BMJ Open 3 (11) (2013) e003471.
[3] World Health Organization, Prevention of Blindness and Visual Impairment, Available from, Priority Eye Diseases, 2015, p. 29 http://www.who.int/blindness/causes/priority/en/index.html.
[4] Royal College of Ophthalmologists, Age-Related Macular Degeneration: Guidelines for Management, The Royal College of Ophthalmologists Scientific Department, London, 2009.
[5] Royal College of Ophthalmologists, Diabetic Retinopathy Guidelines, The Royal College of Ophthalmologists Scientific Department, London, 2012.
[6] J. Caprioli, R. Varma, Intraocular pressure: modulation as treatment for glaucoma, Am J Ophthalmol 152 (3) (2011) 340–344 e2.
[7] H. Nomoto, et al., Pharmacokinetics of bevacizumab after topical, subconjunctival, and intravitreal administration in rabbits, Invest Ophthalmol Vis Sci 50 (10) (2009) 4807–4813.
[8] S.S. Thakur, et al., Intravitreal drug delivery in retinal disease: are we out of our depth? Expert Opin Drug Deliv 11 (10) (2014) 1575–1590.
[9] D.T. Goldenberg, et al., Posterior vitreous detachment with microplasmin alters the retinal penetration of intravitreal bevacizumab (Avastin) in rabbit eyes, Retina 31 (2) (2011) 393–400.
[10] P.J. Missel, Hydraulic flow and vascular clearance influences on intravitreal drug delivery, Pharm. Res. 19 (11) (2002) 1636–1647.
[11] C.G. Wilson, L.E. Tan, J. Mains, Principles of Retinal Drug Delivery from Within the Vitreous, in: U.B. Kompella, H.F. Edelhauser (Eds.), Drug Product Development for the Back of the Eye, Springer, New York, 2011, pp. 125–158.
[12] L.E. Tan, et al., Effects of vitreous liquefaction on the intravitreal distribution of sodium fluorescein, fluorescein dextran, and fluorescent microparticles, Invest. Ophthalmol. Vis. Sci. 52 (2) (2011) 1111–1118.
[13] R.K. Balachandran, V.H. Barocas, Contribution of saccadic motion to intravitreal drug transport: theoretical analysis, Pharm. Res. 28 (5) (2011) 1049–1064.
[14] A. Modareszadeh, et al., Saccade movements effect on the intravitreal drug delivery in vitreous substitutes: a numerical study, Biomech. Model. Mechanobiol. 12 (2) (2013) 281–290.
[15] S. Friedrich, Y.-L. Cheng, B. Saville, Drug distribution in the vitreous humor of the human eye: the effects of intravitreal injection position and volume, Curr. Eye Res. 16 (7) (1997) 663–669.
[16] S. Mitragotri, Healing sound: the use of ultrasound in drug delivery and other therapeutic applications, Nat. Rev. Drug Discov. 4 (3) (2005) 255–260.
[17] M. Nabili, et al., Ultrasound-enhanced delivery of antibiotics and anti-inflammatory drugs into the eye, Ultrasound Med. Biol. 39 (4) (2013) 638–646.
[18] W.-L.L. Suen, et al., Ultrasound-mediated transscleral delivery of macromolecules to the posterior segment of rabbit eye in vivo, Invest. Ophthalmol. Vis. Sci. 54 (6) (2013) 4358–4365.
[19] H. Li, et al., Ultrasound-targeted microbubble destruction enhances AAV-mediated gene transfection in human RPE cells in vitro and rat retina in vivo, Gene Ther. 16 (9) (2009) 1146–1153.
[20] X.-Y. Zhou, et al., Ultrasound-mediated microbubble delivery of pigment epithelium-derived factor gene into retina inhibits choroidal neovascularization, Chin Med. J. (Engl.) 122 (22) (2009) 2711–2717.
[21] F. Stocker, et al., Clinical test for evaluating donor corneas, Arch. Ophthalmol. 84 (1) (1970) 2–7.
[22] H. Weber, et al., The mechanical properties of the vitreous of pig and human donor eyes, Ophthalmic Res. 14 (5) (1982) 335–343.
[23] C.S. Nickerson, et al., Rheological properties of the vitreous and the role of hyaluronic acid, J. Biomech. 41 (9) (2008) 1840–1846.
[24] K. Kobuch, et al., Maintenance of adult porcine retina and retinal pigment epithelium in perfusion culture: characterisation of an organotypic in vitro model, Exp. Eye Res. 86 (4) (2008) 661–668.
[25] S.S. Thakur, H.S. Parekh, Method for preparing a lipid bubble, IP Australia, (2015) Australia.
[26] S.S. Thakur, et al., Stably engineered nanobubbles and ultrasound - An effective platform for enhanced macromolecular delivery to representative cells of the retina, PloS one 12 (5) (2017) e0178305.
[27] B.L. Davis, C.D. Nilson, N. Mamalis, Revised Miyake-Apple technique for post-mortem eye preparation, J. Cataract. Refract. Surg. 30 (3) (2004) 546–549.
[28] R. Neal, et al., Alterations in human vitreous humour following cataract extraction, Exp. Eye Res. 80 (3) (2005) 337–347.
[29] F.A. Bettelheim, J.S. Zigler Jr, Regional mapping of molecular components of human liquid vitreous by dynamic light scattering, Exp. Eye Res. 79 (5) (2004) 713–718.
[30] M. Zhou, et al., Confinement of acoustic cavitation for the synthesis of protein-shelled nanobubbles for diagnostics and nucleic acid delivery, ACS Macro Lett. 1 (7) (2012) 853–856.
[31] I. Sanchez, et al., The parameters of the porcine eyeball, Graefes Arch. Clin. Exp. Ophthalmol. 249 (4) (2011) 475–482.
[32] J. Dua, A. Rana, A. Bhandari, Liposome: methods of preparation and applications, Int. J. Pharm. Stud. Res. 3 (2) (2012) 14–20.
[33] Y. Suh, S. Kang, Acoustic Streaming, in: D. Li (Ed.), Encyclopedia of Microbluidics and Nanofluidics, Springer, New York, 2008, pp. 25–33.
[34] A. Azagury, et al., Ultrasound mediated transdermal drug delivery, Adv. Drug Deliv. Rev. 72 (2014) 127–143.
[35] D. Huang, et al., Ultrasound-mediated nanoparticle delivery across ex vivo bovine retina after intravitreal injection, Eur. J. Pharm. Biopharm. 119 (2017) 125–136.
[36] J.J. Rychak, A.L. Klibanov, J.A. Hossack, Acoustic radiation force enhances targeted delivery of ultrasound contrast microbubbles: in vitro verification, IEEE Trans. Ultrason. Ferroelectr. Freq. Control 52 (3) (2005) 421–433.
[37] M.J. Shortencarier, et al., A method for radiation-force localized drug delivery using gas-filled lipospheres, IEEE Trans. Ultrason. Ferroelectr. Freq. Control 51 (7) (2004) 822–831.
[38] K.W. Ferrara, Driving delivery vehicles with ultrasound, Adv. Drug. Deliv. Rev. 60 (10) (2008) 1097–1102.
[39] G. Moloney, et al., Modified Miyake-Apple camera: illustration of deep anterior lamellar keratoplasty pearls learned from simultaneous anterior and posterior corneal imaging, Cornea 33 (7) (2014) 733–737.
[40] J. Tan, et al., Modification of the Miyake-Apple technique for simultaneous anterior and posterior video imaging of wet laboratory-based corneal surgery, Cornea 33 (3) (2014) 326–330.
[41] M. Nabili, C. Geist, V. Zderic, Thermal safety of ultrasound-enhanced ocular drug delivery: a modeling study, Med. Phys. 42 (10) (2015) 5604–5615.
[42] European Federation, of Societies for Ultrasound in Medicine and Biology, European Committee for Medical Ultrasound Safety Bylaw, Newsletter 12, (1998).
[43] F.A. Bettelheim, T.J. Wang, Dynamic viscoelastic properties of bovine vitreous, Exp. Eye Res. 23 (4) (1976) 435–441.